Science of the Total Environment 932 (2024) 172747

Contents lists available at ScienceDirect

Science of the Total Environment

journal homepage: www.elsevier.com/locate/scitotenv

Application of quasi-empirical orthogonal functions to estimate wildfire impacts in northwestern Spain

Jordina Gili [a,b,*], Mar Viana [a], Philip K. Hopke [c,d]

[a] Institute of Environmental Assessment and Water Research – Spanish Research Council (IDAEA-CSIC), Barcelona, Spain
[b] PhD program of Analytical Chemistry and Environment, University of Barcelona, Barcelona, Spain
[c] University of Rochester School of Medicine and Dentistry, Rochester, NY, USA
[d] Institute for a Sustainable Environment, Clarkson University, Potsdam, NY, USA

HIGHLIGHTS

- In 2022, 18 PurpleAir monitors tracked wildfire smoke's impact on $PM_{2.5}$ in Galicia.
- $PM_{2.5}$ data tested QEOFs from PMF to analyze wildfire smoke's spatial impact.
- 8 factors representing spatial patterns of air pollutants were identified.
- 19 wildfires were linked to peak $PM_{2.5}$ concentrations (>300 μg/m^3; 1-h mean).
- Results identified $PM_{2.5}$ sourcing from wildfires.

GRAPHICAL ABSTRACT

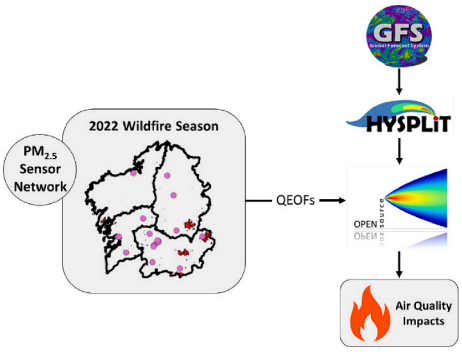

ARTICLE INFO

Editor: Hai Guo

Keywords:
Forest fire
Particulate matter
Smoke
Exposure
Source apportionment

ABSTRACT

Galicia (NW Spain) is one of the most fire-prone regions in Southern Europe. In the summer of 2022, a total of thirteen wildfires each exceeding 500 ha were reported in this area, with ten of these large fires occurring in the Ourense region. To study the impacts of wildfire smoke plumes on ambient air $PM_{2.5}$ concentrations, a network of 18 PurpleAir monitors was deployed across the Galicia region during July and August 2022. The $PM_{2.5}$ concentration data were then used as input to test the applicability of quasi-empirical orthogonal functions (QEOFs obtained with Positive Matrix Factorization (PMF)) to characterize the spatial variability of wildfire smoke impacts on air quality. HYSPLIT back-trajectory analysis and Concentration-Weighted Trajectory (CWT) models were implemented, and the results from these tools were combined with source contributions. As a result, 19 wildfires were identified and linked with peak ambient $PM_{2.5}$ concentrations (>300 μg/m^3 of $PM_{2.5}$; 1-h mean). Specifically, the Folgoso do Courel fire emerged as a significant contributor to these high concentrations and played an important role in influencing a significant number of the identified factors. Moreover, the results also suggested that emissions from fires in Portugal reached the study area, contributing additional impacts on air quality. These results demonstrated that this approach was useful in identifying the emission source areas contributing to observed $PM_{2.5}$ concentrations during wildfire events. The $PM_{2.5}$ concentration maps

* Corresponding author at: Institute of Environmental Assessment and Water Research – Spanish Research Council (IDAEA-CSIC), Barcelona, Spain.
E-mail address: jordina.gili@idaea.csic.es (J. Gili).

https://doi.org/10.1016/j.scitotenv.2024.172747
Received 4 January 2024; Received in revised form 12 April 2024; Accepted 23 April 2024
Available online 26 April 2024

resulting from the CWT analysis were also valuable in understanding the short- and long-term exposures to $PM_{2.5}$ from wildfire smoke.

1. Introduction

The severity of wildfires is increasing, presenting significant environmental, economic, and social threats (Jones et al., 2022). The concept of extreme wildfire events (EWE) has emerged to identify those events with high fire intensity and rapid rates of spread (Duane et al., 2021). In 2022, the South American wildfire season had the highest estimated emissions in the last 20 years, according to the Copernicus Atmosphere Monitoring Service (CAMS). France and Spain were among the most affected European countries, with the highest emissions of wildfire smoke from June to August over the last two decades. Wildfires emit a combination of gaseous compounds, including carbon monoxide (CO), nitrogen oxides (NO_x), non-methane organic compounds (NMOC), and particulate matter (PM) into the atmosphere. However, emissions are highly variable due to differences in fuel, burning conditions, and other environmental factors (Reisen et al., 2015).

Specifically, fine particulate matter (diameter < 2.5 μm; $PM_{2.5}$) generated by wildfires, among other sources, represents a global environmental and public health concern (Burke et al., 2023; Keywood et al., 2015; Kramer et al., 2023). Exposure to wildfire $PM_{2.5}$ has been associated with adverse health effects, including reduced lung function, exacerbation of chronic lung diseases, cardiovascular complications, neurological effects, and increased mortality (Grant and Runkle, 2022; McClure and Jaffe, 2018). Globally, approximately 340,000 annual deaths can be linked to smoke from landscape fires (Johnston et al., 2012).

Actions to mitigate wildfire smoke impacts on public health are contingent on quantifying the actual air pollutant concentrations, which are typically monitored by EU-reference stations. However, isolating $PM_{2.5}$ contributions from wildfire remains unclear (Burke et al., 2023), with few studies comparing health impacts of wildfire-derived air pollution to urban PM (Reisen et al., 2015; Dennekamp et al., 2015; Naeher et al., 2007). Some exposures are sporadic, short-lived, and unpredictable (Henderson et al., 2011; Reisen et al., 2015) and moreover, rural areas experiencing frequent wildfires often lack regulatory monitors, leading to sparse coverage of official reference data. Low-cost air monitors offer improved $PM_{2.5}$ measurement resolution (Kramer et al., 2023), but attributing emission sources, especially wildfires, is essential for understanding and reducing exposure misclassification (Liu et al., 2015).

In aerosol research, receptor modeling by Positive Matrix Factorization (PMF) is widely used for source attribution (Hopke et al., 2020), which has also been linked with back-trajectory analysis (Zhou et al., 2004). Prior studies (Kim and Hopke, 2005; Zhang et al., 2020) have used the representation of air masses to identify the origin of pollutants reaching a given receptor. Once the back trajectories are obtained, the CWT (Concentration Weighted Trajectory; Hsu et al., 2003) method has been widely used to identify emission source areas (Zhang et al., 2019). PMF can be considered as an alternative approach to implementing EOF analysis, particularly when applied to source apportionment tasks since it provides quantitative results. Typical EOF analyses are eigenvector based with mean-centering and normalization using standard deviations that is actually an unweighted least-squares fit in a standardized space. Given that the desired endpoints in our work are quantitative assessments of the wildfire impacts, PMF provides them through an explicit weighted least-squares formalism. Empirical Orthogonal Function (EOF) analysis is frequently used in atmospheric science to decompose a space-time field into spatial patterns (Hannachi et al., 2007) and describe their temporal variability. EOFs extract qualitative information from temporal and spatial data by calculating orthogonal vectors of linear combinations of the original variables. They present the maximum variance contained in the original data (Wilks, 2005). While EOFs are traditionally used for climate and meteorological studies, they may also be used to explore spatial patterns or dominant modes of variability in an air quality dataset with multiple pollutant sources (Henry, 1997a, 1997b, 1997c; Chueinta et al., 2004).

Using this conceptual framework, the uniqueness of this study lies in the utilization of PMF-derived quasi empirical-orthogonal functions (QEOFs) to apportion the spatial distribution of air pollutants. Although the methodologies employed (PMF, EOF, CWT, back trajectories) have been widely documented and independently employed in various studies, this research represents the first instance of their integration and application in wildfire research. Our objective was to identify and quantify wildfire smoke contributions to observed $PM_{2.5}$ concentrations monitored by a network of low-cost PurpleAir monitors during the summer of 2022 in Galicia. If successful, the proposed methodology has the potential to provide improved accuracy of exposure categorization (Alman et al., 2016) and thus improve the links between $PM_{2.5}$ exposures and adverse health outcomes due to wildfires in epidemiological studies (Cascio, 2018; Stowell et al., 2019).

2. Methodology

2.1. Study area

The study area covered the Galicia region (lat. 42° 45′N, long. 7° 41′W) (Fig. S1), located in the northwest (NW) of the Iberian Peninsula. It is one of the regions in Europe with the highest activity of forest fires and, consequently, the most affected by the emissions from this source (Alonso-Betanzos et al., 2003). Historically, a number of extreme wildfires have affected Northern Portugal and Northwestern Spain. The 2017 Iberian wildfires were some of the most severe wildfires and had a significant impact on the region, resulting in human deaths and major economic damage (Chas-Amil et al., 2020). According to the European Forest Fire Information System (EFFIS) (Joint Research Centre, 2023), these wildfires burned an area of about 700,000 ha in total. Another exceptional wildfire season was in Summer 2022 in Spain, where the number of observed fires and the extent of burned area were higher than the average of 2006–2021 (Joint Research Centre, 2023).

Specifically, in Galicia, 50,000 ha were burnt during this period. There are three key factors that make Galicia a fire-prone region. First, the regional climate promotes the accumulation of shrub biomass and consequently, the buildup of flammable forest fuels (Aranha et al., 2020; Fernández-Alonso et al., 2022). As a result, the region exhibits a notable amount of available fuel leading to more intense, rapid combustion when ignited. Furthermore, the flora in Galicia is dominated by Eucalyptus plantations, which are linked to an elevated fire risk (Shakesby and Doerr, 2006; Taylor et al., 2017; Cordero, 2017). The third factor relates to unauthorized fire-setting activities for land management purposes, conducted without prior permissions from the administration. Given these characteristics, coupled with its notable historical fire incidence, Galicia emerged as a favorable study area from which findings may be extrapolated to analogous fire-prone regions.

2.2. Identification of NW Iberian Peninsula wildfires in summer 2022

Thirteen wildfires with >500 ha in area were reported in Galicia during the summer of 2022. Table 1 presents the seven largest wildfires analyzed in this study, and Table S1 (in Supporting Information) provides a full list of the investigated wildfires. The largest of these was the Folgoso do Courel fire (referred to in this work as WF_1), which burned 13,612 ha. Ten other large fires occurred in the Ourense region. The

Table 1
Main wildfire names and total acres burned.

Fire Number	Name	Acres Burned	Initial date	Final date
WF_1	Folgoso do Courel	13,612	14/07/2022	23/07/2022
WF_2	Carballeda de Valdeorras	12,735	15/07/2022	22/07/2022
WF_3	Vilariño do Conso	7,090	15/07/2022	24/07/2022
WF_4	Tresminas*	7,641	17/07/2022	21/07/2022
WF_5	Laza	3,634	10/08/2022	15/08/2022
WF_6	Vilela Seca	3,127	15/07/2022	19/07/2022
WF_7	Verín	2,325	18/07/2022	21/07/2022

* Portugal wildfires.

most significant of these was the Carballeda de Valdeorras fire (WF_2), which started on 15/07/22 and consumed 12,735 ha. It was followed by the Vilariño de Conso fire (7,090 ha; WF_3) as well as the Laza fire (3,634 ha; WF_5), Verín (2,325 ha; WF_7), Verín (2) (917 ha; WF_10), Oímbra (897 ha; WF_11), O Irixo (831 ha; WF_12), Lobeira (640 ha; WF_13) and Carballeda de Valdeorras (2) (594 ha; WF_14). The Caldas de Reis fire (WF_15) in Pontevedra devastated 573 ha, and the Boiro fire (WF_8) burned 2,232 ha. Additionally, large forest fires were reported in Portugal, such as the Tresminas (7,641 ha; WF_4) and Vilela Seca fires (3,127 ha; WF_6) (Joint Research Centre, 2023).

2.3. Site description and data validation

Between June 1 and August 30, we deployed a network of 18 low-cost PurpleAir PA-II outdoor monitors (PA-II-SD; PurpleAir Inc.) across the Galicia region. We selected firefighter stations across Galicia, where the sensors were installed outside the station ensuring unimpaired airflow around them and with a nearby electrical power source. The PurpleAir monitors measure total $PM_{2.5}$ concentration with a $\leq$ 10 s time resolution using 2 Plantower sensors (referred to as channels A and B) in parallel for quality control. The 2-min data were averaged to 1-h values.

To evaluate the performance of the monitors, we conducted an intercomparison of 1-h averaged $PM_{2.5}$ concentrations between PurpleAir and EU-reference equivalent data (Grimm180 laser spectrometer calibrated against EU-reference gravimetric measurements) during a 1-month period at the Barcelona – Palau Reial urban air quality monitoring station prior to the field campaign the intercomparison was repeated after the end of the field campaign. In addition, inter-unit variability was also assessed to determine the consistency between monitors.

Finally, we conducted tests on different data validation and calibration methods, aiming to identify the most optimal data processing protocol for the geographical region (NW Spain) and the main targeted emission source (wildfires). We calculated and evaluate the ALT-CF3 correction developed by Wallace et al. (2021)- by comparing the data from monitor PA17 with the EU-reference data from the Gómez-Franqueira air quality station located in Ourense, Galicia, where this monitor was deployed during the summer period. Furthermore, we tested two US-EPA (Evans et al., 2021) and Barkjohn et al. (2021) correction equations. The CF = Atm and CF = 1 calibration methods provided by Plantower were also explored.

2.4. Back-trajectory calculations

We calculated air parcel back-trajectories using HYSPLIT (Stein et al., 2015) with the GFS 0.25-degree meteorological data set. Five-day back-trajectories with hourly endpoints arriving at each of the 18 receptor sites, at 750 m agl, were calculated for every hour for all of days between June and August 2022.

2.5. Data analysis

In this study, we utilized source apportionment models to assess the impacts of wildfire emissions, utilizing the $PM_{2.5}$ data monitored using a network of 18 low-cost PurpleAir monitors. Specifically, we employed source apportionment methods that rely on the statistical evaluation of $PM_{2.5}$ data collected at receptor sites. Receptor modeling operates based on the principle of mass and species conservation, employing mass balance analysis to identify and allocate sources of airborne PM in the atmosphere (Viana et al., 2008; Hopke, 2010). We used the most frequently employed receptor models (Hopke et al., 2020), Positive Matrix Factorization (PMF), implemented by EPA PMF V5 (Norris et al., 2014) to conduct an Empirical Orthogonal Function (EOF analysis). EOFs uses eigenvector analyses to calculate orthogonal vectors of linear combinations of the original variables, thus capturing the maximum variance contained in the original data (Wilks, 2005). Because PMF does not produce orthogonal vectors, this analysis is considered a quasi-orthogonal empirical function (QEOF) analysis While EOF analyses typically describe spatial patterns, e.g., the spatial variability of meteorological parameters, PMF is typically utilized for source apportionment of samples collected at receptor locations over time. Finally, Concentration-Weighted Trajectory (CWT) analysis focuses on the location of specific emission sources.

The input for the concentration data file for the PMF analysis consisted of the $PM_{2.5}$ data series measured at the 18 PurpleAir monitors between June 1 and August 30, 2022. The input consisted of a matrix of size 1400 × 18, where the values represented the mean hourly $PM_{2.5}$ concentrations for all monitors after applying a correction which was selected at the start of the study (see Section 3.1). Monitors with signal-to-noise ratios (S/N) between 0.5 and 1.0 were defined as weak variables, while those with ratios below 0.5 were categorized as bad and were excluded from the PMF analysis. Thus, monitors PA6, PA12, PA14 and PA16 were classified as weak variables and PA13 was not considered in the analysis. The number of runs used was 20, with seed number 33. From the twenty runs, the convergent run with the minimum Q_{robust} reported by EPA was used for the solutions presented in this study. Additionally, the distribution of scaled residuals for each variable were within ±3, which was considered acceptable according to the literature. PMF was run for solutions ranging between 5 and 9 factors. The uncertainty input matrix was calculated using following equation:

$$\Sigma = 0.15x + \frac{5}{3} \quad (1)$$

where x is the $PM_{2.5}$ measured concentration.

We used back-trajectory analysis and the CWT back trajectory-ensemble model to assess the source emissions contributing to observed $PM_{2.5}$ concentrations during the wildfire events and the accuracy of single-site versus multiple-site methods. Specifically, CWT locates the pollutant source by assigning concentration values at the receptor site to corresponding backward trajectories (Hsu et al., 2003). It is described by the following equation:

$$C_{ij} = \frac{\sum_{l=1}^{M} C_l \tau_{ijl}}{\sum_{l=1}^{M} \tau_{ijl}} \quad (2)$$

where C_{ij} is the average weighted concentration un the grid cell (i, j). Cl is the $PM_{2.5}$ concentration measured at the receptor site, "τ" ijl is the number of trajectory endpoints in the grid cell (i, j) associated with the Cl sample and M is the number of samples that have trajectory endpoints in grid cell (i, j). Eq. (2) is applied to all individual trajectories.

To exclude very short term, local events and to focus on the broader spatial causalities driving the data, we associated trajectories withthe

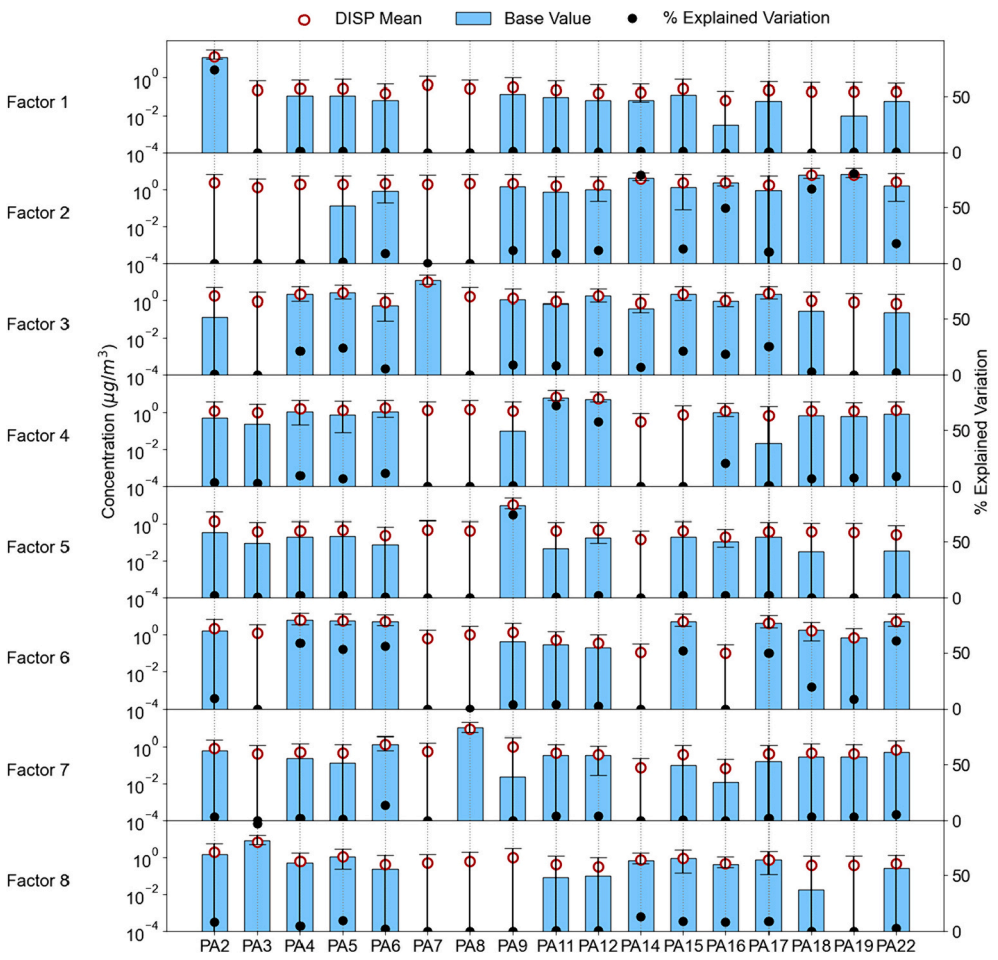

Fig. 1. Source profiles obtained by the PMF (QEOF) analysis of the multiple site $PM_{2.5}$ data.

measured concentration at the receptor site. This association was established using a matrix of reproduced data. This matrix was created by multiplying the factor contributions matrix (G) with the transpose of the factor profiles matrix (F^T).

3. Results and discussion

3.1. Sensor calibration and validation

Results from the intercomparison of $PM_{2.5}$ concentrations from the PurpleAir monitors and the reference instrumentation resulted in $r^2 >$ 0.80 for all of the monitors (Fig. S2) using 1-h time resolution values. The inter-unit variability resulted in $r^2 > 0.99$ (Fig. S3) between each of the monitors and the overall average. Thus, there was comparability among the PurpleAir data across the study region, and it was concluded that the monitors were able to reproduce the temporal variability of aerosol concentrations at an urban background site in Barcelona. However, during the initial intercomparison in Barcelona, the PurpleAir monitors were only challenged with typical urban PM that is substantially different from wildfire smoke. Sensor calibration to represent wildfire emissions was subsequently performed by means of data validation and processing methods.

Fig. S4 shows the mean daily cycle for monitor PA17 (deployed at the local reference monitoring station in Galicia) calculated over a 2-month period (July–August 2022), after processing by applying different calibration methods. A correction factor (CF) was obtained (CF = 3.3) following a methodology inspired by the one proposed by Wallace et al. (2021), which is comparable to the CF obtained by Wallace and Zhao (2023) (CF = 3.4) and to the one recommended by the manufacturer (PurpleAir API; CF = 3). This correction lowers the values and brings them closer to the EU-reference gravimetric measurements. However, the local reference station was not affected by wildfire smoke at the time of the comparison. Therefore, the aerosol mixture was regionally-relevant for our study (from Galicia), but it did not represent wildfire smoke. The Barkjohn et al. (2021) correction provided similar results.

Correlations between the different corrections and the EU-reference data for a 2-month period were calculated. The highest r^2 was obtained for the US-EPA correction (Evans et al., 2021) ($r^2 > 0.83$) followed by the CF = 3.3, CF = 1 and finally the CF = Atm corrections. Therefore, the US-EPA correction (Evans et al., 2021) provided the best approach for the present dataset. One key advantage is that this correction is proposed for wildfire smoke, which is not the case with the calculated correction with local reference data (CF = 3.3; Wallace et al., 2021) Once the optimal data processing protocol was identified, all the data were corrected.

3.2. Air pollution data series

The $PM_{2.5}$ time series plots for each of the 18 study locations are shown in Fig. S5. The majority of the monitors showed data availability >75 %. The lowest data coverage was for monitors PA6, PA7, PA12 and PA13 due to technical limitations mainly linked to disconnection of the sensors from the electrical grid. Mean hourly $PM_{2.5}$ concentrations for all monitors after calibration ranged between <5 and 350 μg/m^3. An hourly maximum of 350 μg/m^3 occurred only at one location for monitor PA2. Hourly $PM_{2.5}$ concentrations generally ranged between 1 and 100 μg/m^3 with higher concentrations measured during the peak episodes that may have coincided with wildfire events.

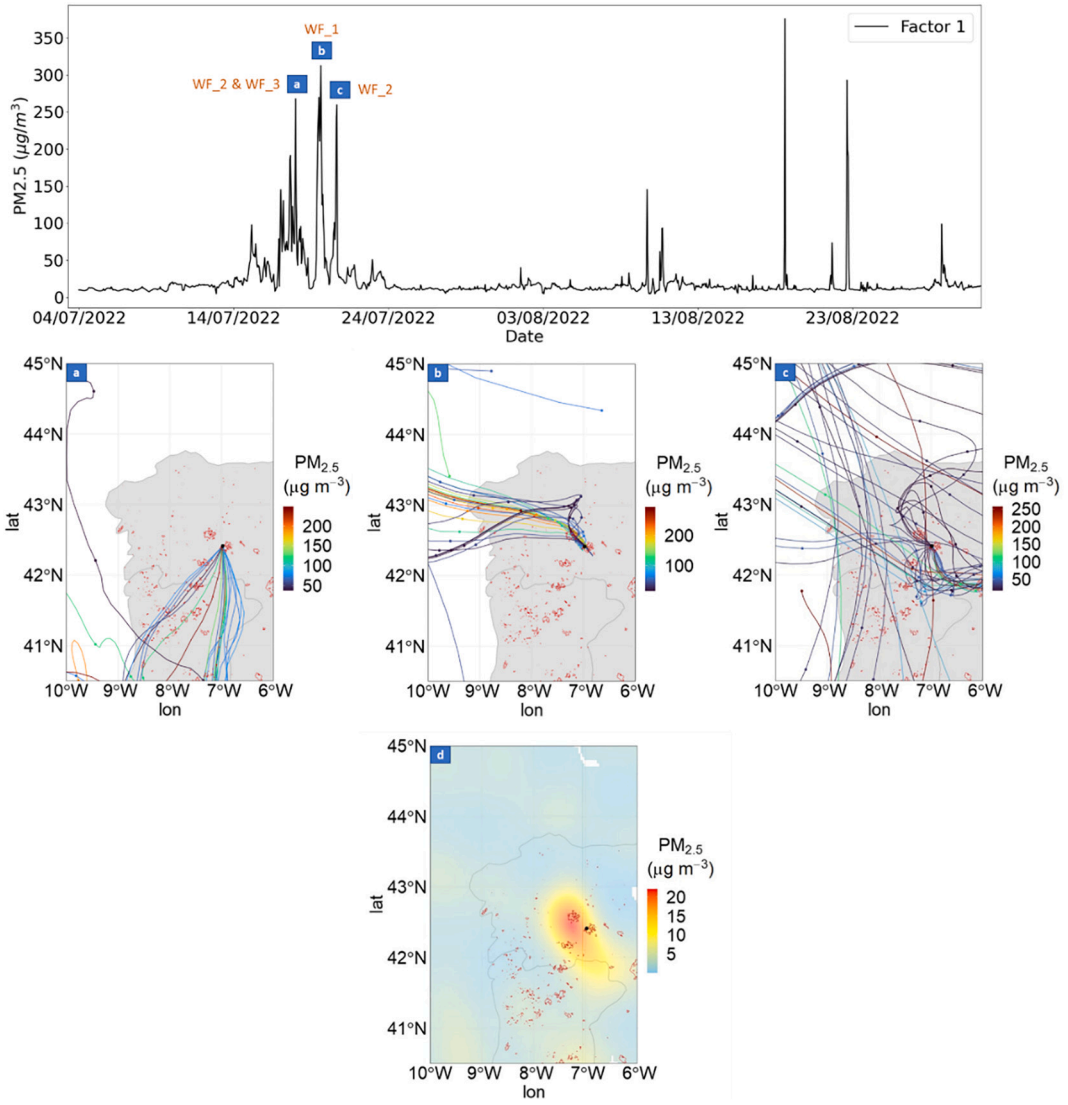

Fig. 2. Plot of the time-series of contributions from Factor 1 (top). Back-trajectory analysis for Factor 1 associated with the $PM_{2.5}$ measured at PA2 (2a, 2b, 2c) (middle) and CWT for Factor 1 for the period 15–24/07/22 (2d) (bottom).

During the sampling period, meteorological conditions played a significant role in the measured $PM_{2.5}$ concentrations. The monitors consistently reported higher values in July compared to August, a difference that can be attributed to weather conditions. According to local weather reports from Meteogalicia (2022b, 2022a), high-pressure systems dominated the region in July. Galicia also experienced an unprecedented heatwave between July 11th and 15th, characterized by extremely hot and dry weather conditions. Precipitation during this time was notably scarce, even nonexistent in regions such as Vigo. These weather conditions significantly hindered the dispersion of atmospheric pollutants, potentially explaining the observed high $PM_{2.5}$ values across all locations in July. These concentrations were considerably higher than those in August, which experienced less stable atmospheric conditions.

3.3. Model results

The PMF analysis was applied with solutions ranging from 5 to 9 factors and examined the resulting solutions. After examining the Q/Q_{exp} quotient, an inflection point at the 8-factor solution was observed, suggesting it might indicate the correct solution for the model. Moreover, solutions with fewer than 7 factors did not adequately capture the spatial patterns described by the $PM_{2.5}$ concentrations recorded across the monitoring network. In the 7-factor solution, PA11, PA12 and PA16 were grouped together, although PA16 explained <50 % of the variance. When considering the 8-factor solution, PA16 was grouped with PA14, PA18 and PA19, had 50 % of the explained variance, and yielded more meaningful interpretations. The 9-factor solution did not provide additional information, and it merely separated the monitors grouped in the Ourense region. Therefore, we selected the 8-factor solution as optimal. It fit the data as shown in the scaled residual plots and was interpretable. Fig. 1 shows the factor profiles describing the relative spatial patterns of the sites. Each factor represents a spatial pattern related to one or several sites that are receiving $PM_{2.5}$ from the same source location, i.e. wildfire (s). To make the contribution time series quantitatively comparable in terms of their magnitude, G-values were normalized by the sum of each factor taken over all of the sites. The time series of G-values describing the mass concentration of that pattern in that given interval, indicating the pattern of possible contributions to the sites across the domain are shown as the top panels in Figs. 2, and 4–10.

3.3.1. Factor 1

Factor 1 mostly represented the $PM_{2.5}$ mass concentrations reported by monitor PA2. In July, the presence of northwesterly back trajectories

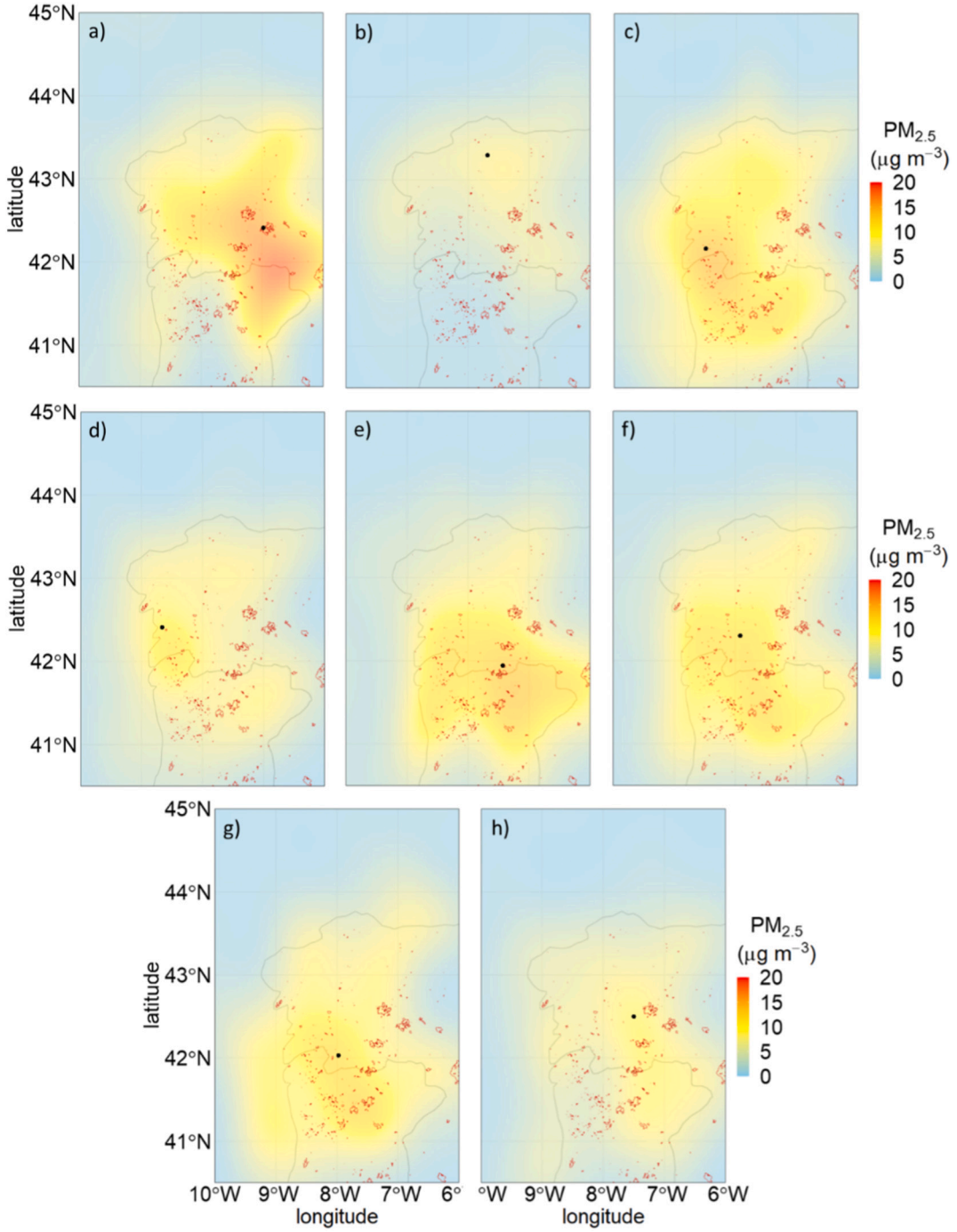

Fig. 3. CWT analysis conducted throughout the entire monitoring period for: a) Factor 1 associated with the $PM_{2.5}$ measured at PA2; b) Factor 2 associated with $PM_{2.5}$ measured at PA14; c) Factor 3 associated with the $PM_{2.5}$ measured at PA7; d) Factor 4 associated with the $PM_{2.5}$ measured at PA11; e) Factor 5 associated with the $PM_{2.5}$ measured at PA9; f) Factor 6 associated with the $PM_{2.5}$ measured at PA4; g) Factor 7 associated with the $PM_{2.5}$ measured at PA8; h) Factor 8 associated with the $PM_{2.5}$ measured at PA3.

suggested that up to >300 µg/m^3 (1 h-mean) of the concentrations monitored by PA2 were related to WF_1 in Folgoso do Courel (Fig. 2b). Furthermore, during July, southerly back trajectories were associated with WF_2 in Carballeda de Valdeorras and WF_3 in Vilariño de Conso fires, where concentrations exceeded 250 µg/m^3 (Fig. 2a, c). These findings are supported by the CWT analysis results, which identified the hotspot located above the aforementioned fires (Fig. 2a). Conversely, results suggested that the remaining peak concentrations monitored in August were linked to short-term local sources (e.g., probably local traffic or other local activities).

The CWT analysis was performed for short-term periods coinciding with the wildfires (Fig. 3d) as well as for the full summer period (Fig. 2a). Results based on the different time resolutions highlight the influence of different emission sources. The wildfire emissions from WF_1–3 are evident for Factor 1 in both maps (Figs. 2d, 3a). However, the map corresponding to the full summer (Fig. 3a) highlights the border area between northern Portugal and Galicia, in close proximity to Bragança (Portugal) as another emission source. This source likely encompasses the influence from industrial activities and traffic emissions originating from Bragança, which impacted the study area driven by

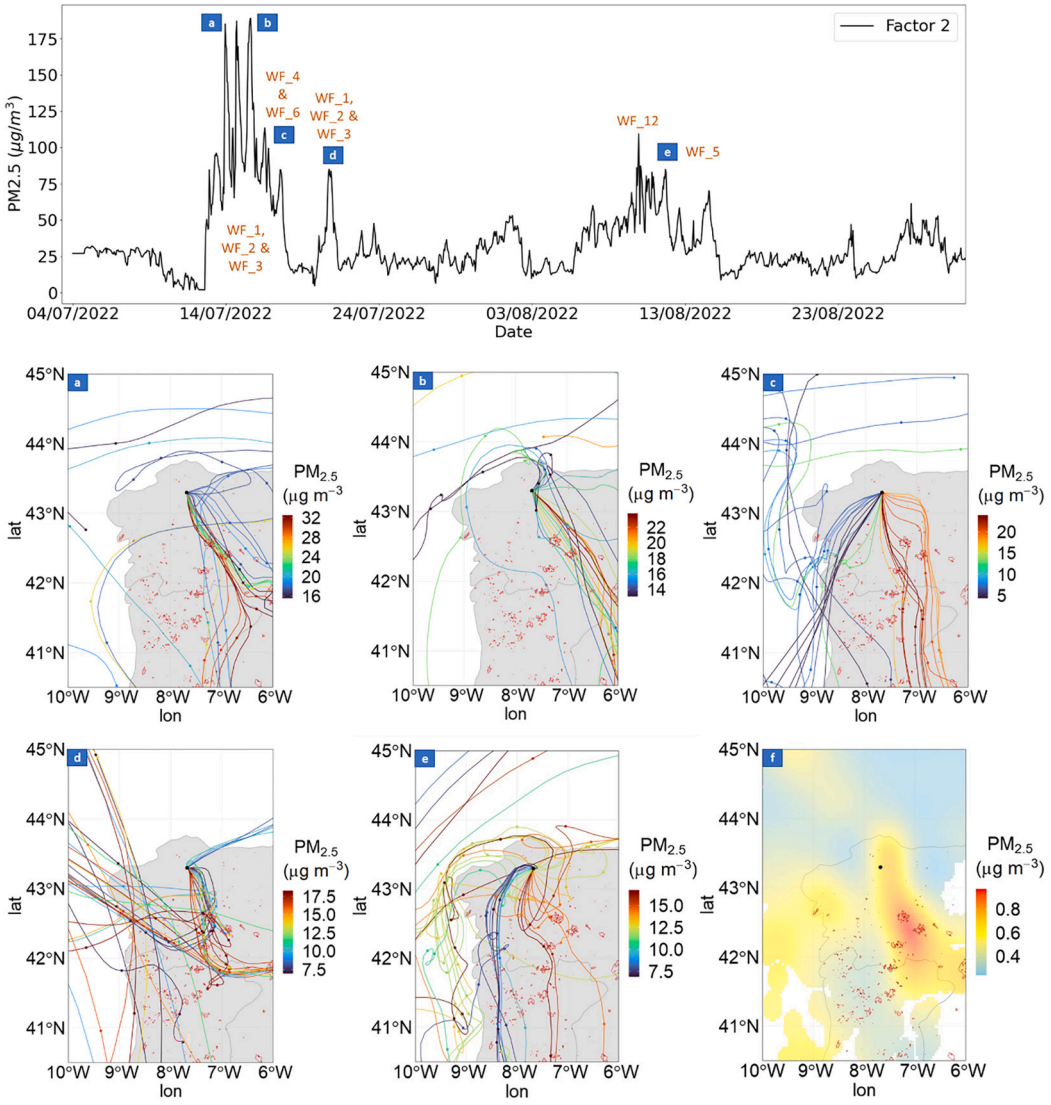

Fig. 4. Plot of time-series of contributions for Factor 2 (top). Back-trajectory analysis for Factor 2 associated with the $PM_{2.5}$ measured at PA14 (4a, 4b, 4c, 4d, 4e) and CWT for the period 20–22/07/22 (4f) (middle and bottom).

southerly winds. These results show the relevance of the CWT mapping at different temporal resolutions with different purposes: the summer average may be useful to evaluate the associations between whole period exposure to $PM_{2.5}$ and wildfire smoke. Conversely, applying CWT to specific dates may prove beneficial when investigating short-term exposures (Cleland et al., 2022; Grant and Runkle, 2022).

In a quantitative analysis, wildfires may have influenced this factor with an increase in mean $PM_{2.5}$ concentrations during the wildfire event of 36 μg/m^3 (with a maximum hourly concentration of 313 μg/m^3) compared to a background level of 14 μg/m^3.

3.3.2. Factor 2

Factor 2 primarily characterizes the $PM_{2.5}$ mass concentrations measured by monitors PA14, PA16, PA18, and PA19. Examining the backward trajectories shown in Fig. 4, it becomes evident that elevated values (>175 μg/m^3) observed from 15 to 18/07/22 were driven by air masses originating relatively constantly from the southeast (Fig. 4a, b, c). Consequently, it is plausible that the smoke plume originating from WF_1, WF_2, and WF_3 may have reached the areas monitored by PA14, PA16, PA18 and PA19 during this time frame. WF_6 in Vilela Seca and WF_4 in Tresminas likely contributed to the observed values as well, especially on 18/07/22. In this case, the back trajectories did not pass over the wildfire regions, but they did pass through the smoke plume as may be observed by NASA Worldview satellite images (NASA, 2024). This result confirms the impact of smoke from these wildfires in the receptor areas, which were reached by back trajectories associated with the monitoring sites related to Factor 2 (Fig. S6). However, on 19/07/22, a significant shift in wind direction resulted in atmospheric cleansing. Nonetheless, on 21/07/22, the return of south-southeastern winds could have once again transported smoke-laden masses from the aforementioned fires, initially affecting PA18 and PA19, and subsequently PA14 and PA16 (Fig. 4d). This last contribution led to potential concentrations of up to 75 μg/m^3 and it is also supported by the CWT map for the corresponding period (Fig. 4f). Furthermore, it is conceivable that the WF_5 in Laza and WF_12 in Irixo may also have played a role in influencing this factor between 10/08/22 and 15/08/22 attaining values up to 75 μg/m^3 (Fig. 4e).

Fig. 3b illustrates the results of the CWT analysis for Factor 2 associated with $PM_{2.5}$ concentrations measured by monitor PA14. This analysis spans the entire monitoring period. As the back-trajectory analysis showed, smoke transport between these sites followed a sequential pattern, initially showing up at PA18 and PA19, and successively reaching PA14 and PA16.

The impact of wildfires in factor 2 increased the mean $PM_{2.5}$

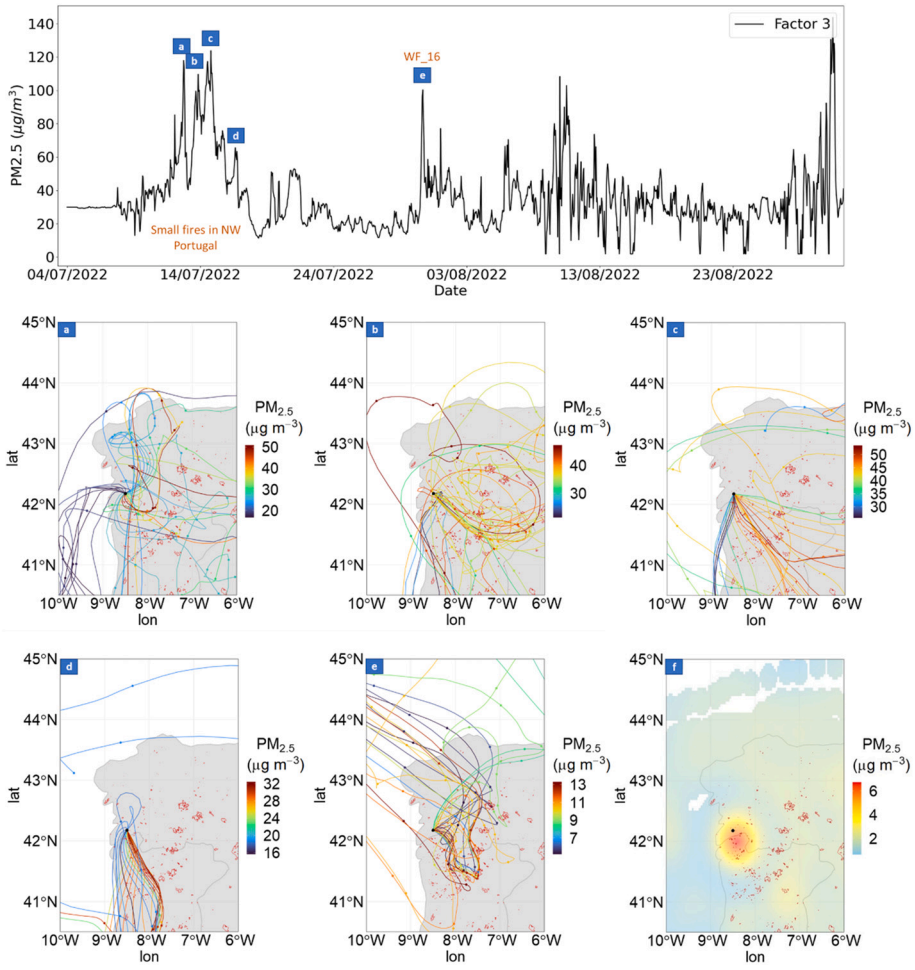

Fig. 5. Plot of time-series of contributions for Factor 3 (top). Back-trajectory analysis for Factor 3 associated with the $PM_{2.5}$ measured at PA7 (5a, 5b, 5c, 5d, 5e) and CWT for the period 13–18/07/22 (5f) (middle and bottom).

concentrations by 36 μg/m^3, with the highest hourly concentration reaching 189 μg/m^3, compared to the baseline level of 24 μg/m^3.

3.3.3. Factor 3

Factor 3 was predominantly associated with the mass concentrations measured by monitor PA7. The CWT analysis shown in Fig. 5f shows that the potential source area for this sensor was situated to the northwest of Portugal where several small fires (<500 ha) ignited on 13/07/22: WF_17 in Lanhelas, WF_19 in Portela and WF_21 in Gondomil e Sanfins. The relevance of these emissions is evident even in the summer average (Fig. 3c). The emissions from these WFs may have contributed to the period of high concentrations (100 μg/m^3) observed in July and driven by southeasterly winds (Fig. 5a, b, c, d). WF_9 in Britelo with an area of 849 ha that burnt on the same day despite being more distant from the site, might also be linked to these high $PM_{2.5}$ concentration periods. Conversely, on 19/07/22, a notable change in wind direction led to cleansing of the trajectory paths. Finally, it is possible that WF_16 in Arbo also played a role in elevating concentrations up to 80 μg/m^3 on the 31/07/22 (Fig. 5e). Notably, from 09 to 31/08/22, the sensor failed to record data, producing a considerable amount of noise in the predicted concentrations.

It has been observed that the influence of wildfires in this factor resulted in a mean increase of 39 μg$PM_{2.5}$/m^3 during the main wildfire event, with the peak hourly concentration reaching 124 μg/m^3, as opposed to the background level of 30 μg/m^3.

3.3.4. Factor 4

Factor 4 mostly describes the $PM_{2.5}$ concentration data measured by PA11 and PA12, both of which were situated in relatively coastal locations. This coastal proximity suggests potential susceptibility to the influence of the land-sea breeze, which can modify the effect of inland emission sources. Similar to the previous factor, the emissions from several small fires (<500 ha) that ignited on 13/07/22 in northwestern Portugal could have contributed to high concentrations (>200 μg/m^3) in July. During this period, air masses originated from the south of the study area (Fig. 6b). This result appears to be confirmed by the hotspot identified by CWT analysis in Figs. 6c and 3d, which also points to northwestern Portugal as a potential source area. However, the highest observed $PM_{2.5}$ concentration (>350 μg/m^3 on 13/07/22) appears to be unrelated to these aforementioned fires as indicated by back-trajectories showing air masses originating from the sea (Fig. 6a). In this case, the land-sea breeze effect might have redirected the influence of inland emission sources. Finally, on 06/08/22 emissions from WF_18 in Pontevedra are likely linked to this factor due to their proximity to the monitoring sites and the south-eastern origin indicated by back trajectories. This connection contributes significantly to concentrations exceeding 50 μg/m^3.

It was observed that wildfires may have caused the mean $PM_{2.5}$ concentrations to rise by 35 μg/m^3 (on average for the main wildfire event), with the maximum hourly concentration reaching 216 μg/m^3, in contrast to the background level of 20 μg/m^3 in this factor.

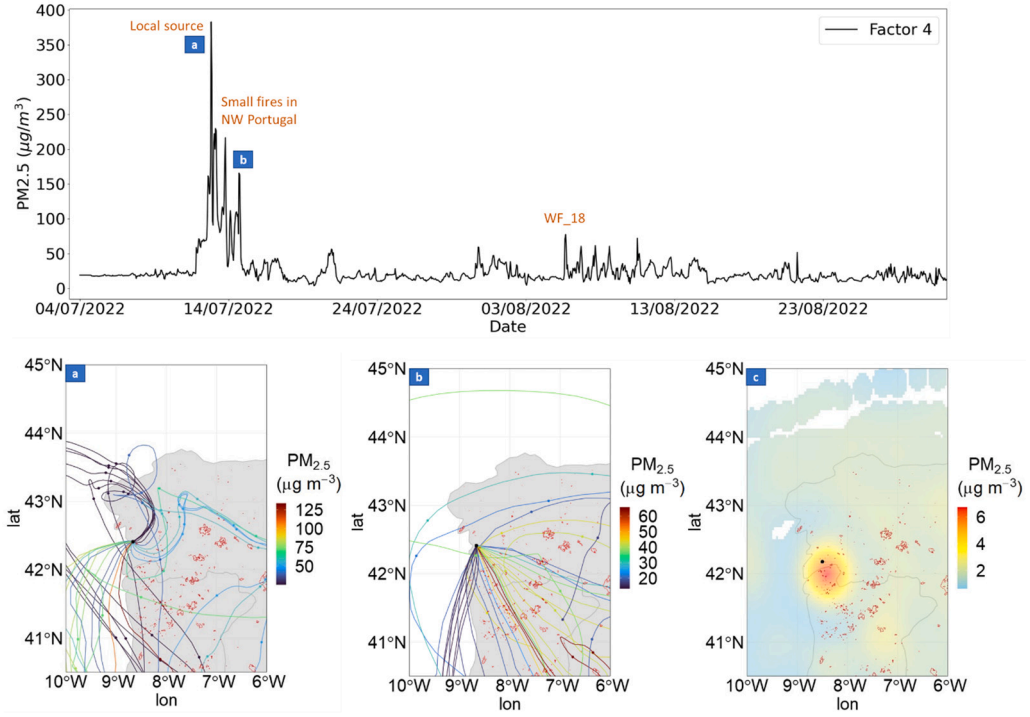

Fig. 6. Plot of time-series of contributions for Factor 4 (top). Back-trajectory analysis for Factor 4 associated with the $PM_{2.5}$ measured at PA11 (6a, 6b) and CWT for the period 13–18/07/22 (6c) (bottom).

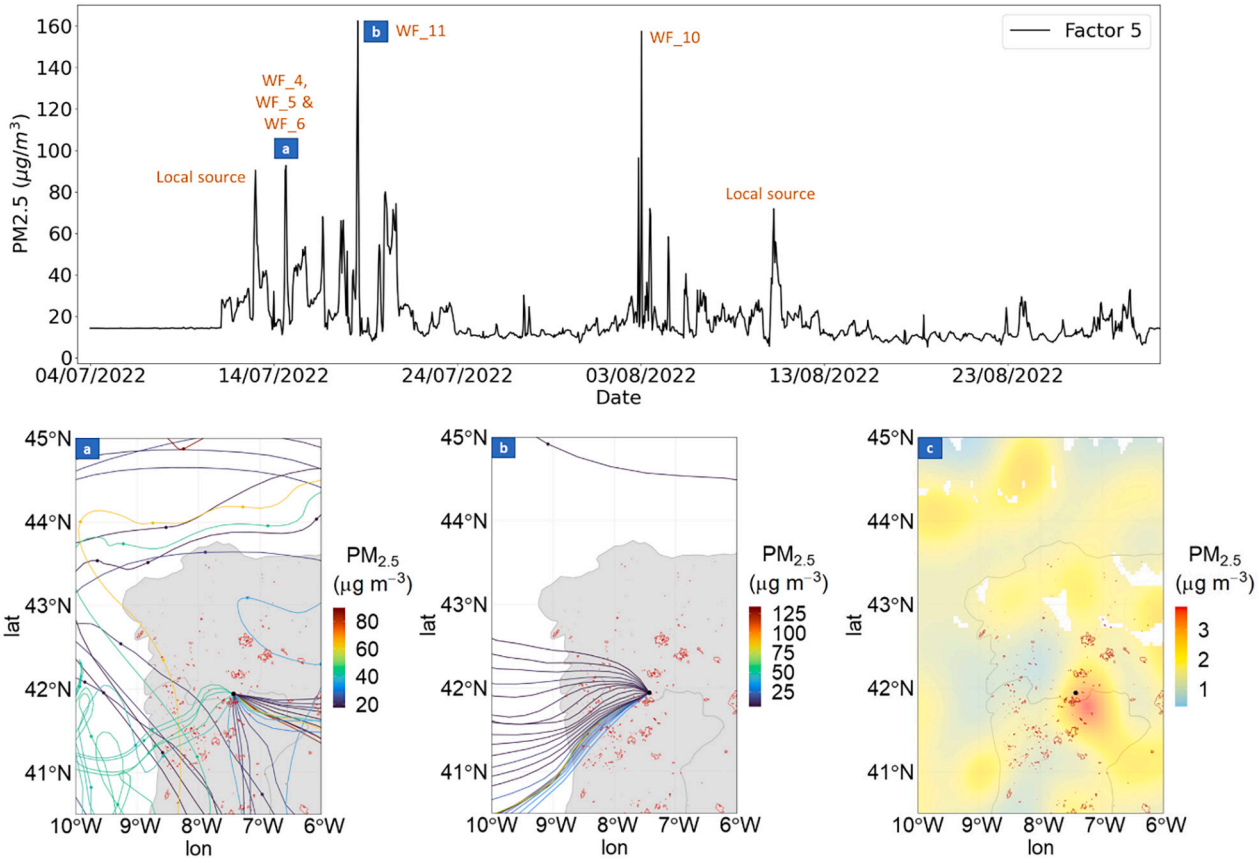

Fig. 7. Plot of time-series of contributions for Factor 5 (top). Back-trajectory and CWT analysis for Factor 5 associated with the $PM_{2.5}$ measured at PA9 (7a, 7b) and CWT for the period 15–19/07/22 (7c) (bottom).

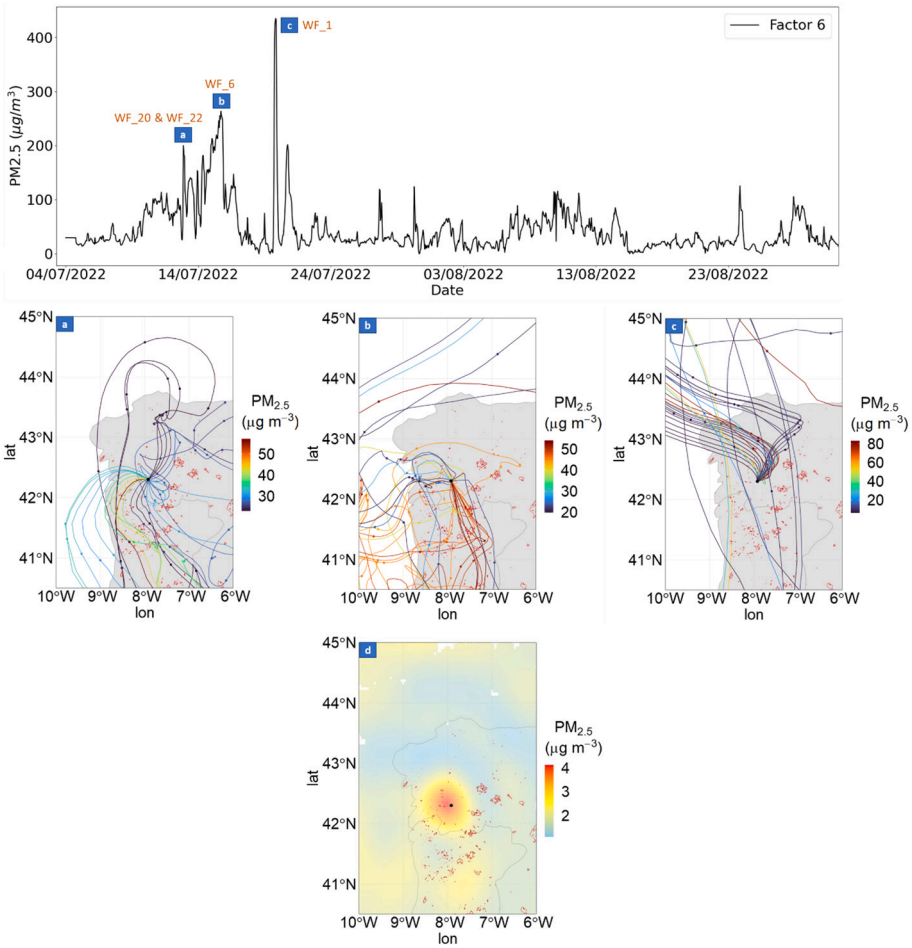

Fig. 8. Plot of time-series of contributions for Factor 6 (top). Back-trajectory and CWT analysis for Factor 6 associated with the $PM_{2.5}$ measured at PA4 (8a, 8b, 8c) (middle) and for the period 13–16/07/22 (8d) (bottom).

3.3.5. *Factor 5*

PA9 exhibited a predominant influence on Factor 5. The results obtained from the CWT analysis (Figs. 7c and 3e) suggest the potential source area was situated in the southeastern region of the PA9 site, spanning across the urban and industrialized zones of northern coast of Portugal. The occurrence of WF_6 in Vilela Seca fire also appears to have significant influence on this factor, particularly when the winds originated from the south-southeast direction during the period from 15 to 18/07/22. This meteorological condition led to air pollutant concentrations reaching 60 μg/m^3 (Fig. 7a). Additionally, on 18/07/22, the contribution of WF_7 in Verín may also likely contributed to this factor. On 19/07/22, a consistent west-southwest wind direction suggests that emissions from WF_4, WF_6, and WF_11 substantially contributed to peak concentrations exceeding 160 μg/m^3 (Fig. 7b).

Furthermore, the proximity of WF_10 to Verín in August likely explains the concentration peak exceeding 150 μg/m^3 observed on 03/08/22. It is plausible that several other instances of elevated pollutant concentrations exceeding 60 μg/m^3 may be attributed to local emission sources.

An increase of 21 μg/m^3 in the mean $PM_{2.5}$ concentrations during the duration of the main wildfire event was observed, with the highest hourly concentration reaching 162 μg/m^3, in comparison to the background level of 12 μg/m^3 in Factor 5.

3.3.6. *Factor 6*

Factor 6 includes a cluster of monitors, specifically PA4, 5, 6, 15, 17, and 22. On 13/07/22, emissions from WF_20 in Melón and WF_22 in Ribadavia probably contributed to the increased $PM_{2.5}$ concentrations observed in this factor's contributions, especially when air masses originated from the southwest (Fig. 8a). During the period 15–16/07/22, the transect of the southeasterly back trajectories, passing through WF_6, likely resulted in pollutant concentrations reaching 200 μg/m^3 (Fig. 8b) as also shown in the CWT map corresponding to this time period (Fig. 8d). The presence of back trajectories originating from the northeast of the monitoring sites was likely associated with the smoke from WF_1 and WF_3, as supported by the NASA Worldview observation (NASA, 2024) on 20/07/2022 (Fig. S6). This led to the highest concentration recorded for this factor, exceeding 400 μg/m^3 (Fig. 8c). The results derived from the CWT analysis indicated that the potential source region for this factor was situated in the central part of northern Portugal, primarily driven by southeasterly air masses (Fig. 3f).

The impact of wildfires in Factor 6 is evident in a 63 μg/m^3 increase in the mean $PM_{2.5}$ concentration, with the highest hourly concentration reaching 435 μg/m^3, contrasting with the background level of 34 μg/m^3.

3.3.7. *Factor 7*

Factor 7 was primarily driven by monitor PA8. The CWT analysis conducted for the entire monitoring period (Fig. 3g) shows similarities to the CWT analysis for Factor 6, indicating that this monitor also received emissions from northern Portugal. However, there is a notable difference in that PA8 was likely affected by emissions from WF_13 in Lobeira on 24/08/22 (Fig. 9b). The advection of air masses passing through this wildfire may be associated with concentrations up to >50 μg/m3 at the monitoring site. CWT map corresponding to this time period (Fig. 9c) also points WF_13 as a potential source. Furthermore, during early August, the divergent directions of back trajectories related

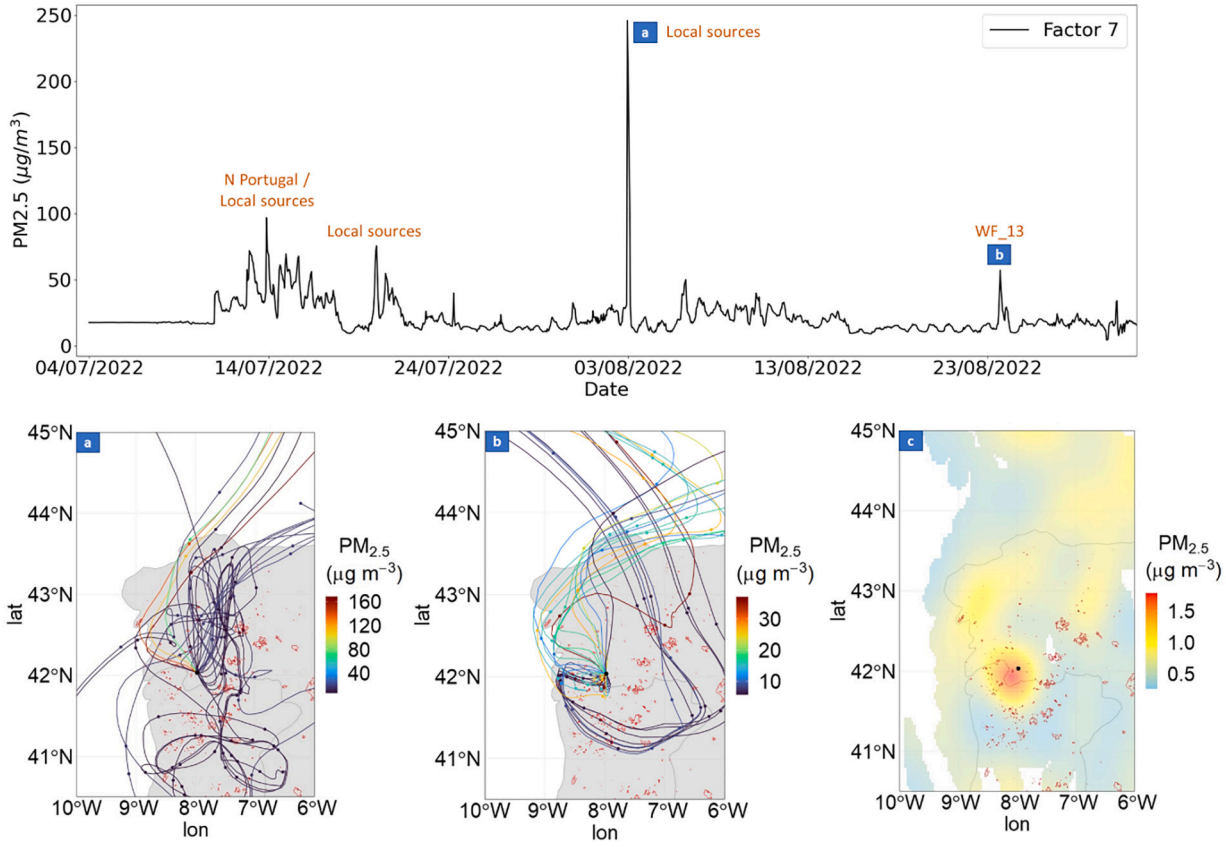

Fig. 9. Plot of time-series of contributions for Factor 7 (top). Back-trajectory analysis for Factor 7 associated with the $PM_{2.5}$ measured at PA8 (9a, 9b) and CWT for the period 24–26/08/22 (9c) (bottom).

to the highest concentrations recorded by PA8 suggest that a local source may be the primary contributor affecting this monitor (Fig. 9a).

In this factor, wildfires may have contributed to an increase in the mean concentration during the main wildfire event by 24 μg$PM_{2.5}$/m^3, with the peak hourly concentration reaching 97 μg/m^3, compared to the background level of 19 μg/m^3.

3.3.8. *Factor 8*

Factor 8 was dominated by PA3. The high values of the CWT analysis were driven by the presence of southwesterly air masses, indicating source areas in northeastern Portugal (Fig. 3h). Notably, the transect of the south-southeasterly back trajectories between 16 and 18/07/22, passing through the WF_3 region, likely contributed to $PM_{2.5}$ concentrations reaching 150 μg/m^3 (Fig. 10a, b, d, e). Additionally, emissions from WF_1 may have been a source when air masses originated from the northeast of the sensor site on 20/07/22, leading to the highest values measured by PA3 (Fig. 10c). These results were consistent with those from the CWT map (Fig. 10f). Several other observed values with concentrations exceeding 50 μg/m^3, may be attributed to emissions from local sources.

It appears that wildfires may have caused a 25 μg$PM_{2.5}$/m^3 increase in the mean concentration during the wildfire event, with the maximum hourly concentration peaking 219 μg/m^3, as opposed to the background level of 19 μg/m^3 in Factor 8.

4. Summary and conclusions

Source apportionment of wildfire emissions contributing to $PM_{2.5}$ concentrations was performed using PMF combined with back-trajectory analysis and concentration-weighted trajectory (CWT) analysis. The impacts from several of the major wildfires were detected as high $PM_{2.5}$ concentrations across the study area. WF_1 in Folgoso do Courel, the largest fire that occurred during the study period, contributed to a significant number of factors (four factors). Alternatively, WF_6 in Vilela Seca was linked to three factors, showing that the emissions from fires in Portugal reached Galicia. This pattern was also observed for WF_4 in Tresminas, located even further to the south of Galicia. WF_3 in Vilariño de Conso affected three factors. Despite its considerable size, WF_2 in Carballeda de Valdeorras appeared to only affect Factor 1, which was strongly associated with the PA2 site. Finally, smaller fires also contributed to the high concentrations observed at nearby monitoring sites.

In terms of impact, wildfires led to an increase in background levels ranging from on average 21 to 39 μg/m^3 for the duration of the wildfire events (from 5 to 10 days) for all factors except Factor 6, where the increase was 63 μg/m^3, with a maximum hourly peak concentration reaching 435 μg/m^3.

We conclude that the use of the PMF-derived quasi-empirical orthogonal functions (QEOFs) to apportion the spatial distribution of air pollutants provided robust results and facilitated identifying 8 factors representing spatial patterns associated with one or multiple sites affected by the same specific wildfire. The use of a network of low-cost monitors proved useful in quantifying the effects of wildfires on air quality and identifying potential source areas. These results may be valuable for short and long-term epidemiologic studies and health impact assessment studies.

CRediT authorship contribution statement

Jordina Gili: Writing – original draft, Visualization, Software, Investigation, Formal analysis, Data curation, Conceptualization. **Mar Viana:** Supervision, Resources, Methodology, Investigation,

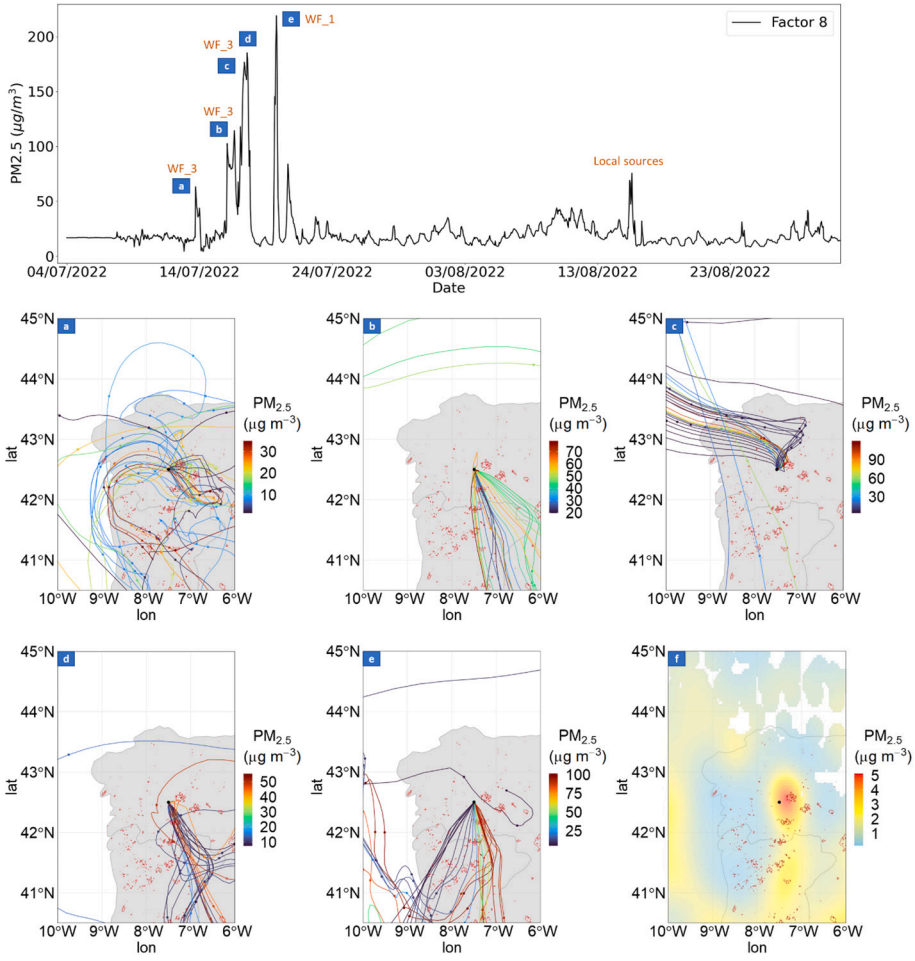

Fig. 10. Plot of time-series of contributions for Factor 8 (top). Back-trajectory and CWT analysis for actor 8 associated with the $PM_{2.5}$ measured at PA3 (10a, 10b, 10c, 10d, 10e) and CWT for the period 16–20/07/22 (10f) (middle and bottom).

Conceptualization. **Philip K. Hopke:** Supervision, Software, Resources, Methodology, Investigation, Formal analysis, Conceptualization.

Declaration of competing interest

The authors declare that they have no known competing financial interests or personal relationships that could have appeared to influence the work reported in this paper.

Data availability

Data will be made available on request.

Acknowledgements

The authors gratefully acknowledge the accessibility, technical support and active collaboration of Dirección Xeral de Defensa do Monte of Xunta de Galicia and Universidade da Coruña. Furthermore, the authors' appreciation extends to the Dirección Xeral de Calidade Ambiental, Sostenibilidade e Cambio Climático and Generalitat de Catalunya for providing access to air quality data. The authors are also grateful to Achim J. Latz for the scientific and technical support provided to run and optimize back-trajectory calculations.

Funding sources

This work was carried out in the framework of projects of FIRE-RES (https://fire-res.eu/), Horizon 2020 research and innovation programme under grant agreement No. 101037419, Severo Ochoa Project (CEX2018-000794-S) and project 2017SGR41 (AGAUR).

Appendix A. Supplementary data

Supplementary data to this article can be found online at https://doi.org/10.1016/j.scitotenv.2024.172747.

References

Alman, B.L., Pfister, G., Hao, H., Stowell, J., Hu, X., Liu, Y., Strickland, M.J., 2016. The association of wildfire smoke with respiratory and cardiovascular emergency department visits in Colorado in 2012: a case crossover study. In: Environmental Health: A Global Access Science Source, 15, p. 64. https://doi.org/10.1186/s12940-016-0146-8.

Alonso-Betanzos, A., Fontenla-Romero, O., Guijarro-Berdiñas, B., Hernández-Pereira, E., Paz Andrade, M.I., Jiménez, E., Soto, J.L.L., Carballas, T., 2003. An intelligent system for forest fire risk prediction and firefighting management in Galicia. Expert Syst. Appl. 25, 545–554. https://doi.org/10.1016/S0957-4174(03)00095-2.

Aranha, J., Enes, T., Calvão, A., Viana, H., 2020. Shrub biomass estimates in former burnt areas using sentinel 2 images processing and classification. Forests 11, 555. https://doi.org/10.3390/F11050555.

Barkjohn, K.K., Gantt, B., Clements, A.L., 2021. Development and application of a United States-wide correction for PM2.5 data collected with the PurpleAir sensor. Atmos. Measure. Techn. 14, 4617–4637. https://doi.org/10.5194/amt-14-4617-2021.

Burke, M., Childs, M.L., de la Cuesta, B., Qiu, M., Li, J., Gould, C.F., Heft-Neal, S., Wara, M., 2023. The contribution of wildfire to PM2.5 trends in the USA. Nature 622, 761–766. https://doi.org/10.1038/s41586-023-06522-6.

Cascio, W.E., 2018. Wildland fire smoke and human health. Sci. Total Environ. 624, 586–595. https://doi.org/10.1016/j.scitotenv.2017.12.086.

Chas-Amil, M.L., García-Martínez, E., Touza, J., 2020. Iberian Peninsula October 2017 wildfires: burned area and population exposure in Galicia (NW of Spain). Int. J. Disaster Risk Reduction 48, 101623. https://doi.org/10.1016/j.ijdrr.2020.101623.

Chueinta, W., Hopke, P.K., Paatero, P., 2004. Multilinear model for spatial pattern analysis of the measurement of haze and visual effects project. Environ. Sci. Technol. 38, 544–554.

Cleland, S.E., Wyatt, L.H., Wei, L., Paul, N., Serre, M.L., Jason West, J., Henderson, S.B., Rappold, A.G., 2022. Short-Term Exposure to Wildfire Smoke and PM2:5 and Cognitive Performance in a Brain-Training Game: A Longitudinal Study of U.S. Adults. Environmental Health Perspectives 130, 6. https://doi.org/10.1289/EHP10498.

Cordero, A., 2017. Large scale eucalypt plantations associated to increased fire risk. PeerJ Prepr. 5 https://doi.org/10.7287/peerj.preprints.3348v1.

Dennekamp, M., Straney, L.D., Erbas, B., Abramson, M.J., Keywood, M., Smith, K., Sim, M.R., Glass, D.C., Del Monaco, A., Haikerwal, A., Tonkin, A.M., 2015. Forest fire smoke exposures and out-of-hospital cardiac arrests in Melbourne, Australia: a case-crossover study. Environ. Health Pers. 123, 959–964. https://doi.org/10.1289/ehp.1408436.

Duane, A., Castellnou, M., Brotons, L., 2021. Towards a comprehensive look at global drivers of novel extreme wildfire events. Clim. Change 165, 43. https://doi.org/10.1007/s 10584-021-03066-4.

Evans, R., Larkin, S., Barkjohn, K.J., Clements, A., Holder, A., 2021. EPA tools and resources, webinar, AirNow fire and smoke map: extension of the US-wide correction for purple $PM_{2.5}$ sensors. Office of Research and Development. https://www.epa.gov/sites/default/files/2021-05/documents/toolsresources-webinar_purpleairsmoke_210519b.pdf.

Fernández-Alonso, J.M., Llorens, R., Sobrino, J.A., Ruiz-González, A.D., Alvarez-González, J.G., Vega, J.A., Fernández, C., 2022. Exploring the potential of Lidar and Sentinel-2 data to model the post-fire structural characteristics of Gorse Shrublands in NW Spain. Remote Sens. (Basel) 14, 6063. https://doi.org/10.3390/rs14236063.

Grant, E., Runkle, J.D., 2022. Long-term health effects of wildfire exposure: a scoping review. J. Climate Change Health 6, 100110. https://doi.org/10.1016/j.joclim.2021.100110.

Hannachi, A., Jolliffe, I.T., Stephenson, D.B., 2007. Empirical orthogonal functions and related techniques in atmospheric science: a review. Int. J. Climatol. 27, 1119–1152. https://doi.org/10.1002/joc.1499.

Henderson, S.B., Brauer, M., MacNab, Y.C., Kennedy, S.M., 2011. Three measures of forest fire smoke exposure and their associations with respiratory and cardiovascular health outcomes in a population-based cohort. Environ. Health Perspect. 119, 1266–1271. https://doi.org/10.1289/ehp.1002288.

Henry, R.C., 1997a. Receptor model applied to patterns in space (RMAPS). J. Air Waste Manage Assoc. 47, 216–219.

Henry, R.C., 1997b. Receptor model applied to patterns in space (RMAPS) part II-apportionment of airborne particulate sulfur from project MOHAVE. J. Air Waste Manage Assoc. 47, 220–225.

Henry, R.C., 1997c. Receptor Model Applied to Patterns in Space (RMAPS) Part III–Apportionment of Airborne Particulate Sulfur in Western Washington State, 47, pp. 226–230.

Hopke, P.K., 2010. The application of receptor modeling to air quality data. Pollut. Atmospher. 91–109.

Hopke, P.K., Dai, Q., Li, L., Feng, Y., 2020. Global review of recent source apportionments for airborne particulate matter. Sci. Total Environ. 740, 140091 https://doi.org/10.1016/j.scitotenv.2020.140091.

Hsu, Y.-K., Holsen, T.M., Hopke, P.K., 2003. Comparison of hybrid receptor models to locate PCB sources in Chicago. Atmos. Environ. 37, 545–562.

Johnston, F.H., Henderson, S.B., Chen, Y., Randerson, J.T., Marlier, M., DeFries, R.S., Kinney, P., Bowman, D.M.J.S., Brauer, M., 2012. Estimated global mortality attributable to smoke from landscape fires. Environ. Health Perspect. 120, 695–701. https://doi.org/10.1289/ehp.1104422.

Joint Research Centre, 2023. European Forest Fire Information System (EFFIS). Retrieved October 28, 2023. https://effis.jrc.ec.europa.eu/.

Jones, M.W., Abatzoglou, J.T., Veraverbeke, S., Andela, N., Lasslop, G., Forkel, M., Smith, A.J.P., Burton, C., Betts, R.A., van der Werf, G.R., Sitch, S., Canadell, J.G., Santín, C., Kolden, C., Doerr, S.H., Le Quéré, C., 2022. Global and regional trends and drivers of fire under climate change. Rev. Geophysics 60, e2020RG000726. https://doi.org/10.1029/2020RG000726.

Keywood, M., Cope, M., Meyer, C.P.M., Iinuma, Y., Emmerson, K., 2015. When smoke comes to town: the impact of biomass burning smoke on air quality. Atmos. Environ. 121, 13–21. https://doi.org/10.1016/j.atmosenv.2015.03.050.

Kim, E., Hopke, P.K., 2005. Identification of fine particle sources in mid-Atlantic us area. Water Air Soil Pollution 168, 391–421. https://doi.org/10.1007/s11270-005-1894-1.

Kramer, A.L., Liu, J., Li, L., Connolly, R., Barbato, M., Zhu, Y., 2023. Environmental justice analysis of wildfire-related $PM_{2.5}$ exposure using low-cost sensors in California. Sci. Total Environ. 856, 159218 https://doi.org/10.1016/j.scitotenv.2022.159218.

Liu, J.C., Pereira, G., Uhl, S.A., Bravo, M.A., Bell, M.L., 2015. A systematic review of the physical health impacts from non-occupational exposure to wildfire smoke. Environ. Res. 136, 120–132. https://doi.org/10.1016/j.envres.2014.10.015.

McClure, C.D., Jaffe, D.A., 2018. US particulate matter air quality improves except in wildfire-prone areas. PNAS 115, 7901–7906. https://doi.org/10.1073/pnas.1804353115.

Meteogalicia, 2022a. INFORME CLIMATOLÓXICO MES DE AGOSTO DE 2022. https://www.meteogalicia.gal/datosred/infoweb/clima/informes/estacions/informesestacionais/2022/202202_gl.pdf.

Meteogalicia, 2022b. INFORME CLIMATOLÓXICO MES DE XULLO DE 2022. https://www.meteogalicia.gal/datosred/infoweb/clima/informes/estacions/mensuais/2022/202207_gl.pdf.

Naeher, L.P., Brauer, M., Lipsett, M., Zelikoff, J.T., Simpson, C.D., Koenig, J.Q., Smith, K. R., 2007. Woodsmoke health effects: a review. Inhalation Tox. 19, 67–106. https://doi.org/10.1080/08958370600985875.

NASA, 2024. NASA Worldview. Retrieved March 1, 2024. https://worldview.earthdata.nasa.gov.

Norris, G., Duvall, R., Brown, S., Bai, S., 2014. EPA Positive Matrix Factorization (PMF) 5.0 Fundamentals and User Guide. U.S. Environmental Protection Agency, Washington, DC. EPA/600/R-14/108 (NTIS PB2015-105147).

Reisen, F., Duran, S.M., Flannigan, M., Elliott, C., Rideout, K., 2015. Wildfire smoke and public health risk. Int. J. Wildland Fire 24, 1029–1044. https://doi.org/10.1071/WF15034.

Shakesby, R.A., Doerr, S.H., 2006. Wildfire as a hydrological and geomorphological agent. Earth Sci. Rev. 74, 269–307. https://doi.org/10.1016/j.earscirev.2005.10.006.

Stein, A.F., Draxler, R.R., Rolph, G.D., Stunder, B.J.B., Cohen, M.D., Ngan, F., 2015. NOAA's HYSPLIT atmospheric transport and dispersion modeling system. Bull. Amer. Meteor. Soc. 96, 2059–2077. https://doi.org/10.1175/BAMS-D-14-00110.1.

Stowell, J.D., Geng, G., Saikawa, E., Chang, H.H., Fu, J., Yang, C.E., Zhu, Q., Liu, Y., Strickland, M.J., 2019. Associations of wildfire smoke PM2.5 exposure with cardiorespiratory events in Colorado 2011-2014. Environ. Int. 133, 105151 https://doi.org/10.1016/j.envint.2019.105151.

Taylor, K.T., Maxwell, B.D., McWethy, D.B., Pauchard, A., Nuñez, M.A., Whitlock, C., 2017. Pinus contorta invasions increase wildfire fuel loads and may create a positive feedback with fire. Ecology 98, 678–687. https://doi.org/10.1002/ecy.1673.

Viana, M., Kuhlbusch, T.A.J., Querol, X., Alastuey, A., Harrison, R.M., Hopke, P.K., Winiwarter, W., Vallius, M., Szidat, S., Prévôt, A.S.H., Hueglin, C., Bloemen, H., Wåhlin, P., Vecchi, R., Miranda, A.I., Kasper-Giebl, A., Maenhaut, W., Hitzenberger, R., 2008. Source apportionment of particulate matter in Europe: a review of methods and results. J. Aerosol Sci. 39, 827–849. https://doi.org/10.1016/j.jaerosci.2008.05. 007.

Wallace, L., Zhao, T., 2023. Spatial variation of PM2.5 indoors and outdoors: results from 261 regulatory monitors compared to 14,000 low-cost monitors in three Western states over 4.7 years. Sensors 23, 4387. https://doi.org/10.3390/s23094387.

Wallace, L., Bi, J., Ott, W.R., Sarnat, J., Liu, Y., 2021. Calibration of low-cost PurpleAir outdoor monitors using an improved method of calculating $PM_{2.5}$. Atmos. Environ. 256, 118432 https://doi.org/10.1016/j.atmosenv.2021.118432.

Wilks, D.S., 2005. Statistical Methods in the Atmospheric Sciences, Second edition. Academic Press, Burlington, MA, p. 648.

Zhang, K., Zhou, L., Fu, Q., Yan, L., Bian, Q., Wang, D., Xiu, G., 2019. Vertical distribution of ozone over Shanghai during late spring: a balloon-borne observation. Atmos. Environ. 208, 48–60. https://doi.org/10.1016/j.atmosenv.2019.03.011.

Zhang, K., Xu, J., Huang, Q., Zhou, L., Fu, Q., Duan, Y., Xiu, G, 2020. Precursors and potential sources of ground-level ozone in suburban Shanghai. Front. Environ. Sci. Eng. 14, 92. https://doi.org/10.1007/s11783-020-1271-8.

Zhou, L., Hopke, P.K., Liu, W., 2004. Comparison of two trajectory based models for locating particle sources for two rural New York sites. Atmos. Environ. 38, 1955–1963. https://doi.org/10.1016/j.atmosenv.2003.12.034.